Performance Evaluation of iPVC™ Fitting with Turner Lock Gasket

Submitted to:

PPI Pipe
1085-11, Boedeul-ro, Jangan-myeon
Hwaseong-city
Gyeonggi-do, Korea

by

T. D. O'Rourke
J. Strait
C. Atkins

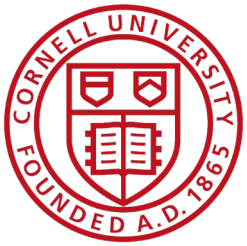

Cornell University
School of Civil and Environmental Engineering
Cornell University
Hollister Hall
Ithaca, NY 14853
August, 2022

Acknowledgements

The authors wish to recognize the excellent effort of Cornell graduate and undergraduate students who made these experiments successful. Namely, the contributions of Sam Allen and Kian Sorhaindo are gratefully acknowledged.

Table of Contents

List of Figures

List of Tables

Section 1

Introduction

This report is submitted to PPI Pipe (herein referred to as PPI). It presents full-scale test results from a program to investigate the direct tension and compression performance of an iPVC™ fitting with Turner Lock gasket (herein referred to as iPVC™ fitting) connected to nominal 6 in. (150 mm) diameter DR 18, AWWA C 900 iPVC pipe (AWWA, 2007) pipes. The purpose of the testing is to evaluate the load capacity, leakage, and load vs. displacement characteristics of an iPVC™ fitting joined to iPVC pipes under both axial elongation and compression. The work was undertaken in the Cornell Large Scale Lifelines Testing Facility, which is part of the Bovay Laboratory Complex at Cornell University.

The report is organized into five sections. Section 1 provides introductory remarks. Section 2 presents the key characteristics of the iPVC™ fitting that was tested in addition to summarizing the stress vs strain results of tensile coupon tests performed on the iPVC material. Section 3 provides the results of two direct axial tension tests. Section 4 provides the results of one direct axial compression test. Section 5 summarizes the test results.

Section 2
iPVC™ Fitting

2.1. Introduction

This section of the report describes the iPVC™ fitting, which is used to join two iPVC pipes. Figure 2.1 provides a longitudinal cross-section through one of the iPVC™ fittings with key measurements performed as part of this investigation. The iPVC™ is essentially two iPVC bells connected by a cylinder with smaller cross-sectional area than that of the IPVC spigots inserted at each side of the fitting.

The internal diameter and wall thickness of the iPVC pipe used in this study was measured at four locations around the circumference. The average internal diameter = 5.52 in. (140 mm) and average wall thickness = 0.53 in. (13 mm), from which the average outside diameter = 6.57 in. The transverse cross-sectional area = 10 in.^{2} (6400 mm^2).

Following PPI's instructions, the forward edge of each spigot was beveled by a belt sander over a distance of approximately 0.38 in. (9.7 mm). Each spigot was beveled at 15° relative to the horizontal from the back end of the bevel.

Figure 2.2 a shows a transverse cross-section of the iPVC™ fitting, with the internal diameter of the bell of the iPVC™ = 6.72 in. (171 mm). A black gasket sits inside an indentation, or raceway, around the inside circumference. Attached to the gasket are 12 sets of teeth. Figure 2 b is a close up of the gasket and teeth. The teeth are inclined in the forward direction. As the pipe spigot is inserted, the exterior pipe surface moves past the teeth without incurring penetration. When the direction of movement is reversed, the inclined teeth penetrate the pipe wall and generate resistance to pullout. The spigot was inserted into the iPVC™ fitting bell until a black circle on the external spigot surface lined up with the end of the bell. The black circle is provided for each iPVC spigot to control longitudinal penetration of the iPVC™ fitting.

This section also presents some results of axial tensile coupon testing for the iPVC pipe material, as reported by Price et al. (2018). Tensile coupon specimens were cut and machined from nominal 6-in. (150-mm)-diameter pipe sections and tested in accordance with the ASTM–E8 2013 Standard (ASTM, 2013).

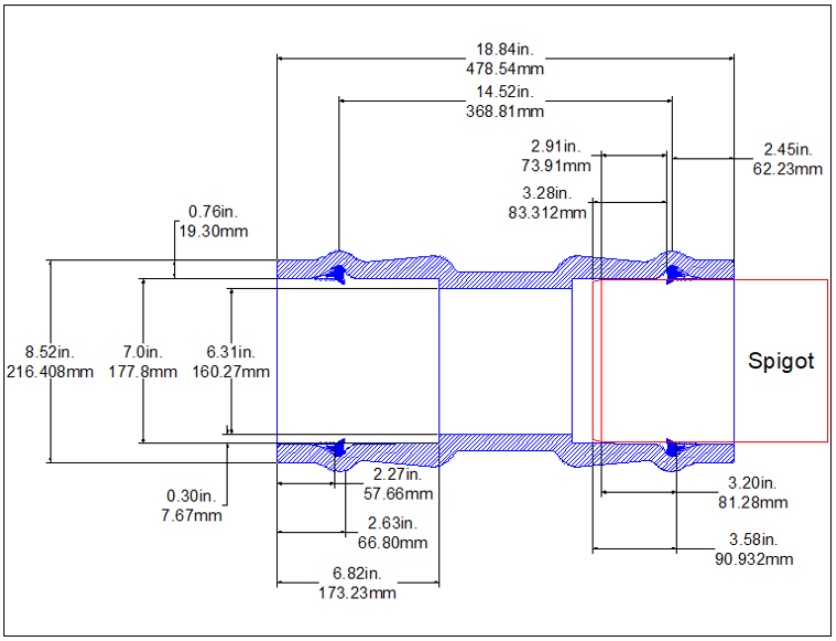

Figure 2.1 Longitudinal Profile of iPVC™ Fitting

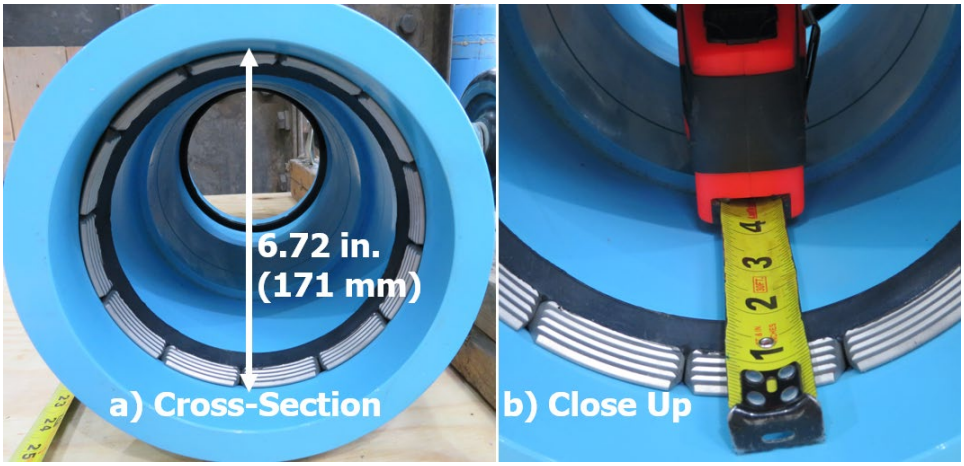

Figure 2.2 Transverse Cross-Section of iPVC™ Fitting

2.2. Stress vs. Strain Data

Only a brief description of the stress vs strain data is presented herein, and the reader is referred to Price et al. (2018) for more detail. The uniaxial stresses vs. axial strains measured from clip-on extensometers for three PVC specimens from iPVC pipe are shown in Figure 2.3. An expanded view of stress vs. strain data is shown in Figure 2.4, in which the axial strain gage measurements were used to plot stress vs. strain as it extends just beyond the elastic range. Table 2.1 provides a

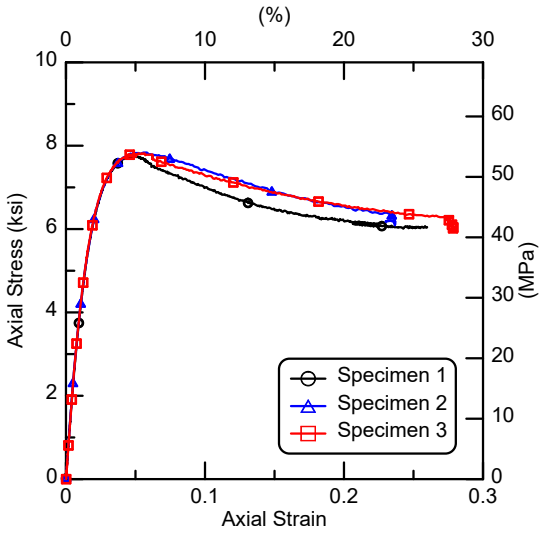

Figure 2.3. Stress vs. Strain Curve to Failure Using Clip-On Extensometer

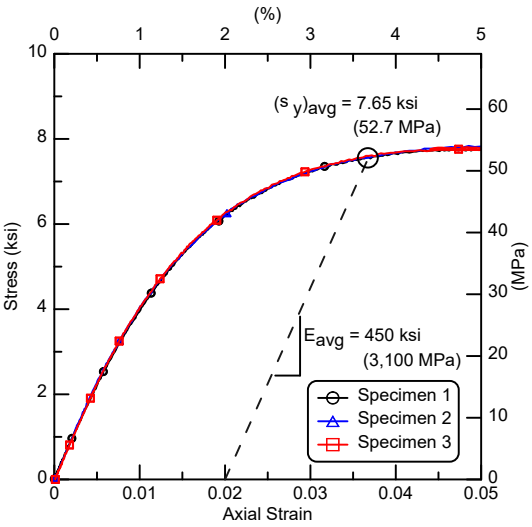

Figure 2.4. Average Young's Modulus and Yield Stress

Table 2.1. Summary of Properties from Tensile Coupons

		Specimen			**Average**	Standard Deviation
		1	2	3		
Young's Modulus, E	ksi	446	457	448	**450.3**	5.86
	(GPa)	(3.08)	(3.15)	(3.09)	**(3.1)**	(0.04)
Offset Yield, σ_y	ksi	7.6	7.6	7.6	**7.6**	0.02
	(MPa)	(52.3)	(52.4)	(52.1)	**(52.3)**	(0.1)
Peak Tensile Strength	ksi	7.8	7.8	7.8	**7.8**	0.042
	(MPa)	(53.5)	(54.1)	(53.9)	**(53.8)**	(0.29)
Peak Tensile Strain	%	4.9	4.9	5.2	**5.0**	0.21
Ultimate Tensile Strength	ksi	6.0	6.1	6.0	**6.0**	0.036
	(MPa)	(41.6)	(42)	(41.5)	**(41.7)**	(0.25)
Ultimate Tensile Strain	%	26	24	28	**26**	2
Poisson's Ratio, ν		N/A^1	0.37	0.38	**0.38**	0.007

summary of the Young's modulus, yield stress, peak tensile stress and strain, ultimate tensile stress and strain, and Poisson's ratio determined from the tensile coupon specimens.

Section 3
iPVC™ Fitting Tension Tests

This section summarizes the results of two direct tension tests on iPVC™ fittings, each joined to two iPVC pipe specimens. The tension test was performed under internal water pressure that is typical of water distribution systems. The tests are used to evaluate the axial pull-out capacity as well as the load vs. displacement characteristics of the iPVC™ fitting connected to two iPVC pipes.

3.1. Set Up for First Tension Test

Figure 3.1 shows a plan view of the setup and equipment for the first axial tension test. A 55-kip (245-kN) MTS actuator with 6 in. (150 mm) of stroke, load cell, and load frame were used to apply tensile load to the test specimen. An iPVC™ fitting, as described in Section 2, was connected to two nominal 6 in. (150 mm) diameter DR 18, AWWA C 900 iPVC pipes provided by PPI. The test specimen was fitted at either end with end caps to allow for internal pressurization during loading. The orientation of the test specimen is shown with respect to north (N) and south (S).

A photo of the test setup is shown in Figure 3.2. The figure shows the iPVC™ fitting and gripping collars near both the north and south ends of the test specimen. A series of three Stargrip® Gen2 restraining collars were used at either end of the specimen to transfer load from the actuator and loading frame to the specimen. The three restraining collars acted as a grip for the pipes during axial load application. Four 0.75 in. (19 mm) threaded rods, spanning the restraining collars, carried the tensile force. The test specimen is oriented in the figure so that north is to the right. Both north and south joints of the iPVC™ fitting are shown in the figure.

Table 3.1 lists the instrumentation for the first tension and compression test according to name, description, and location. Each specimen consisted of two sections of pipe joined by an iPVC™ fitting. The strain gage stations, each with 8 strain gages, were located at the center of the iPVC™ fitting and at distances both 24 in. (610 mm) north and south of the iPVC™ center. At each plane the gages were located at the 12, 3, 6, and 9 o´clock positions (crown, east springline, invert, and west springline, respectively). Both longitudinal and circumferential strains were measured at each gage location.

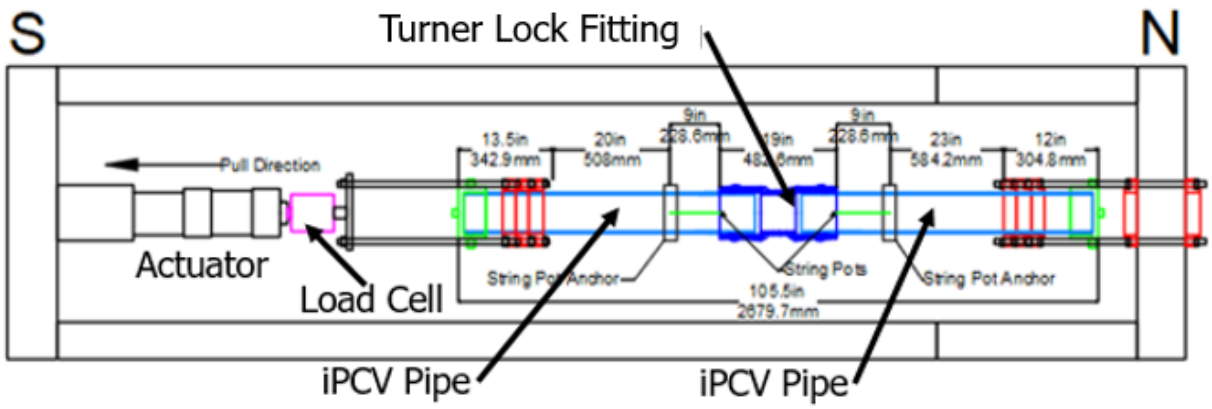

Figure 3.1. Plan View of Axial Tension Test

Figure 3.2. Test Specimen in the Direct Tension Frame

Displacements were measured with horizontal string potentiometers (string pots) and by the actuator. A flow meter was used to monitor the ingress and egress of water with respect to the test specimen. Pressure transducers measured internal water pressure. Axial load was measured by a load cell connected to the actuator, with a loading rate of 1 in./min. (25 mm/min.).

After the specimen was instrumented and centered in the test frame the test was initiated by starting the data acquisition and laboratory hydraulic systems. The data sampling rate was 5 Hz.

Table 3.1. Instrumentation for First Tension/Compression Test of iPVC™ Fitting

Location	Instrument Description	Local Instrument Name
24 in. North of Centerline	Crown, Bi-Axial Strain	24CC 24CA
	Invert, Bi-Axial Strain	24IC 24IA
	East, Bi-Axial Strain	24EC 24EA
	West, Bi-Axial Strain	24WC 24WA
Centerline	Crown, Bi-Axial Strain	0CA
		0CC
	Invert, Bi-Axial Strain	0IA
		0IC
	East, Bi-Axial Strain	0EA
		0EC
	West, Bi-Axial Strain	0WA
		0WC
24 in. South of Centerline	Crown, Bi-Axial Strain	-24CC
		-24CA
	Invert, Bi-Axial Strain	-24IC
		-24IA
	East, Bi-Axial Strain	-24EC
		-24EA
	West, Bi-Axial Strain	-24WC
		-24WA
Pipe Clamp, 3 in. North Crown of Centerline	Horizontal String Pot	3C_HSP
Pipe Clamp, 3 in. North Invert of Centerline	Horizontal String Pot	3I_HSP
Pipe Clamp, 3 in. North East of Centerline	Horizontal String Pot	3E_HSP
Pipe Clamp, 3 in. North West of Centerline	Horizontal String Pot	3W_HSP
Pipe Clamp, -3 in. South Crown of Centerline	Horizontal String Pot	-3C_HSP
Pipe Clamp, -3 in. South Invert of Centerline	Horizontal String Pot	-3I_HSP
Pipe Clamp, -3 in. South East of Centerline	Horizontal String Pot	-3E_HSP
Pipe Clamp, -3 in. South West of Centerline	Horizontal String Pot	-3W_HSP
Magnet clamp, North End-cap	Horizontal String Pot	N_Slip
Magnet clamp, South End-cap	Horizontal String Pot	S_Slip
North End-cap	Flow Meter	Flow Meter
Testing Deck	Pressure Transducer	Pressure_Deck
North End_cap	Pressure Transducer	Pressure_Pipe
Actuator	Actuator Displacement	MTS_Disp_IN
Actuator, Centerline	Horizontal String Pot	MTS_Disp_EX
Load Cell	Force Transducer	Force

The loading restraints at either end of the specimen were tightened to avoid end movement due to pressurization. The test was performed under displacement control. Displacement was applied until the specimen was no longer capable of holding internal water pressure.

3.2. Internal Pressure for First Tension Test

Approximately 80 psi (550 kPa) of internal water pressure was applied during the first tension test. Figure 3.3 presents the pressure plotted relative to time. Initially the pressure spiked to nearly 90 psi (620 kPa), then air was bled from the test specimen. Most of the time the pressure remained steady at approximately 80 psi (550 kPa). During the application of tensile load the iPVC™ fitting and adjoining pipes were expanding axially and thus reducing the pressure. In response, the pressure was increased automatically through the introduction of additional water, providing an average pressure of about 78 psi (536 kPa). At the end of the test, the spigot pulled past the north joint seal, causing leakage and pressure loss. In the plot, various labels and arrows point toward a part of the pressure vs. time plot.

3.3. Force and Displacement for First Tension Test

Figure 3.4 presents a plot of the load vs. net displacement of the north joint, for which net displacement is the displacement corrected for the elastic elongation of the pipe between the locations of the string pot anchors and the gripping teeth of the iPVC™ fitting. The elastic displacement correction to obtain the net displacement was relatively small at about 0.05 in. (1.3 mm). The net displacement is the actual movement of the iPVC™ fitting joint without any elastic extension of the pipe and iPVC™ fitting. Virtually all the net movement was concentrated at the north joint. The south joint moved a maximum of approximately 0.35 in. (8.9 mm).

Labels for various events are presented in Figure 3.3 A maximum load of 20.4 kips (90.7 kN) occurred at 0.7 in. (18.0 mm). A crack formed along the knit line of the iPVC™ fitting near the maximum load. Teeth began to pull from the north joint at displacements ranging from 1 in. (25 mm) to about 2 in. (50 mm). The teeth pulled out of the north joint at approximately 2.2 in. (56 mm). A close examination of the data and video of the iPVC™ fitting during testing shows that movement occurred rapidly from about 2.5 in. (64 mm) to greater than 4 in. (102 mm). At about 4.0 in. (102 mm) the north spigot pulled past the gasket in the north joint, when substantial and uncontrollable leakage occurred. This displacement is consistent with the dimensions in Figure

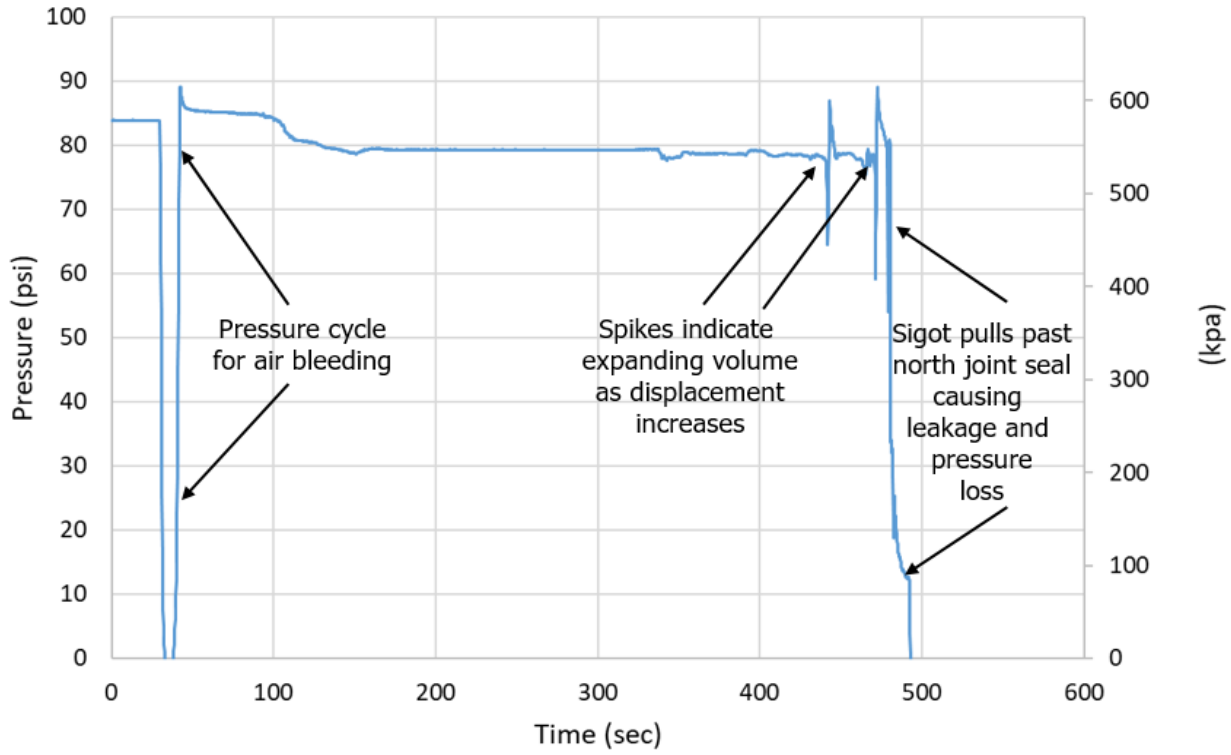

Figure 3.3 Internal Pressure vs. Time for First Tension Test

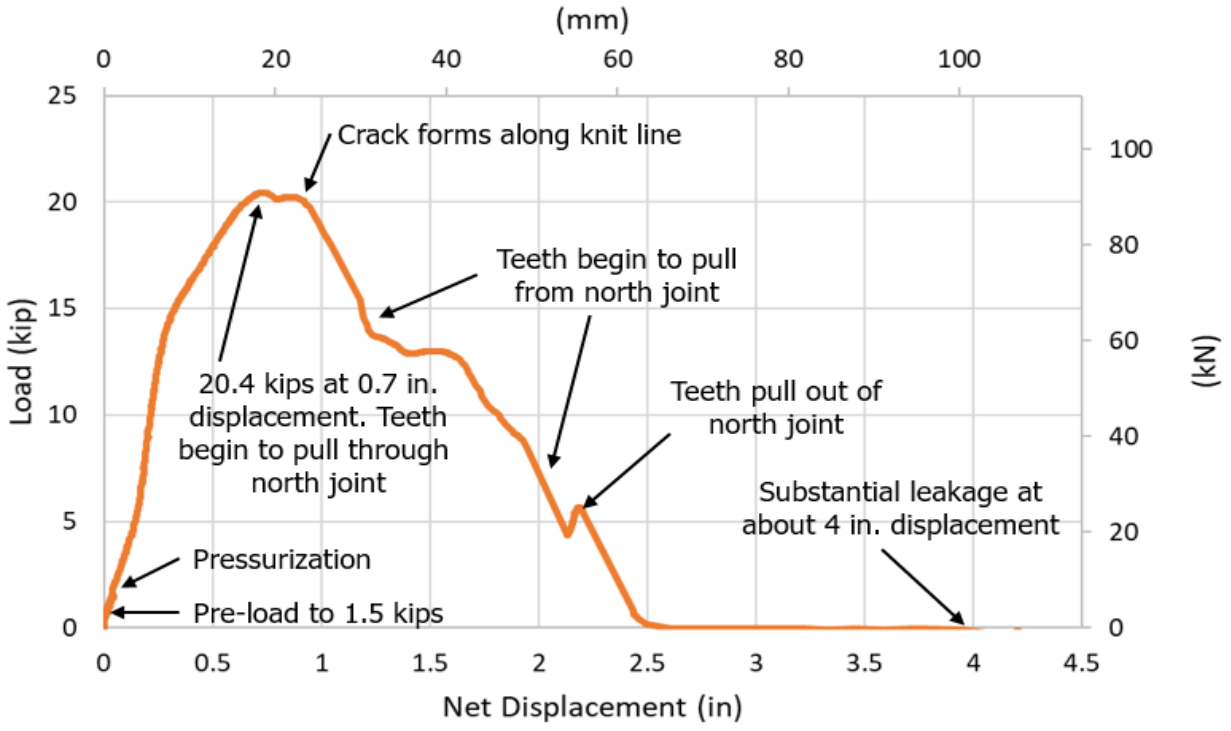

Figure 3.4 Axial Load vs. Net Displacement of North Joint for First Tension Test

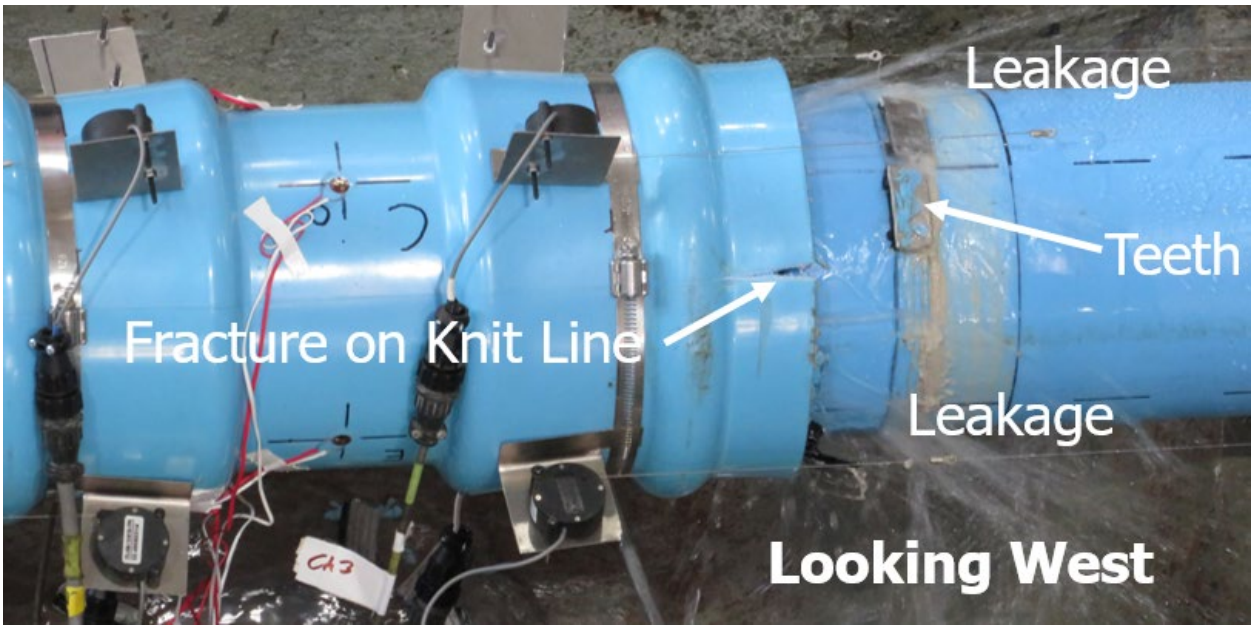

Figure 3.5 Photo of Leaking iPVC™ Fitting for First Tension Test

2.1 that show a distance of about 3.64 in. (92 mm) between the end of the spigot and the gasket center. A north joint net displacement of approximately 4.00 in. (107 mm) was actually measured when high leakage was initiated. This movement was large enough to carry the end of the spigot past the gasket in the north joint.

Figures 3.5 and 3.6 provide photographs of the leaking and failed iPVC™ fitting, looking west and east, respectively. Figure 3.4 shows the fracture along the knit line of the fitting. Some teeth were adhered to the barrel of the spigot. Figure 3.5 shows teeth that had accumulated in the basin (to catch leakage) beneath the iPVC™ fitting. These photos show that the teeth were separated from the gasket, which remained at the location of the indentation, or raceway, of the fitting. Pullout of the north spigot was accompanied by separation between the teeth and gasket. The gasket maintained its pressure seal until the end of the spigot was displaced to the outside end of the gasket.

3.4. Strains and Forces for First Tension Test

As previously discussed, strain gages were located at the center of the iPVC™ fitting and at distances both 24 in. (610 mm) north and south of the iPVC™ fitting center. A direct comparison

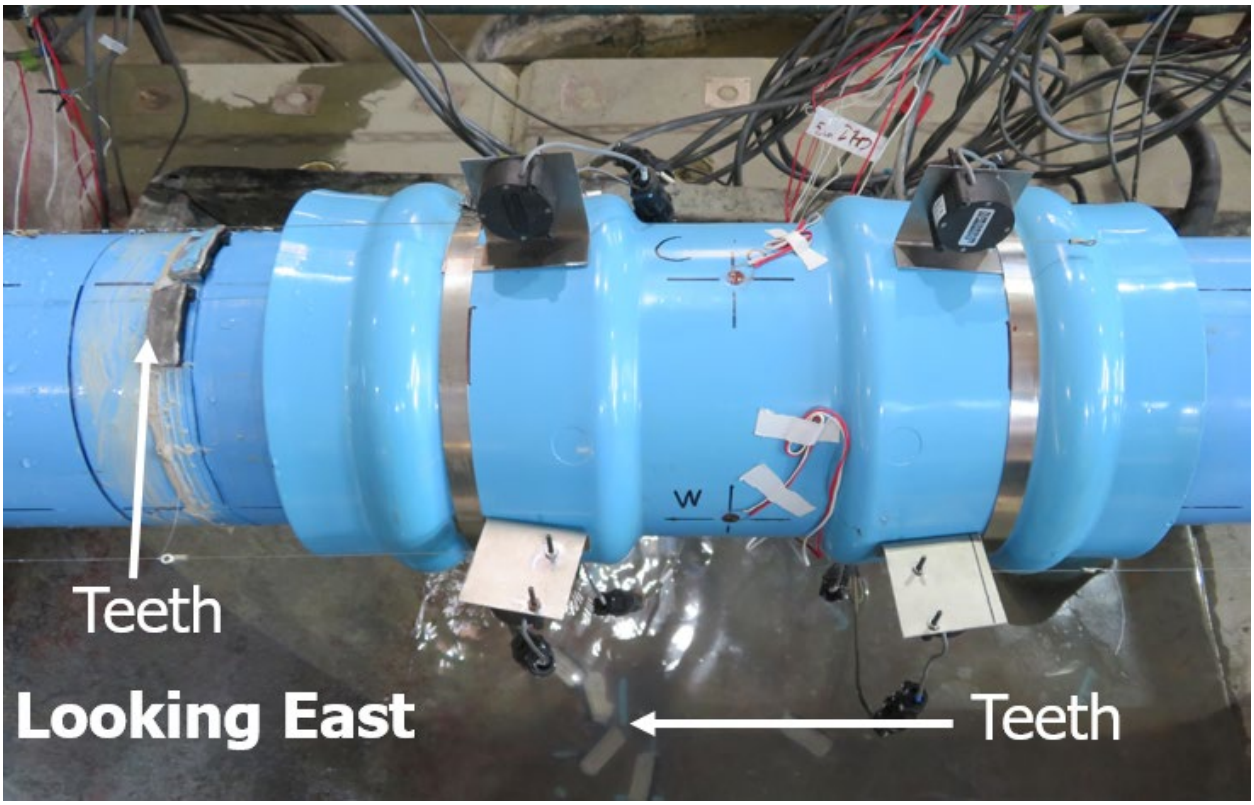

Figure 3.6 Photo of Failed iPVC™ Fitting for First Tension Test

shows that the increase in axial force evaluated by the strain gages agreed within 10 % of the load measured by the load cell using the properties of the iPVC material summarized by Price et al. (2018). Strain gage readings were converted to stresses that clearly showed preloading, pressurization, axial tension, and reduction in pressure to zero. The stresses were consistent with theoretical stresses, assuming linear elastic properties as summarized by Price et al. (2018).

3.5. Set Up for Second Tension Test

The test setup and equipment for the second axial tension test were very similar to those shown in Figures 3.1 and 3.2. The description previously provided for the first tension test applies also for the second tension test, and the reader is referred to Section 3.1 for a detailed description of the test procedures and setup. Table 3.2 lists the instrumentation for the second tension test according to name, description, and location. The instrumentation differed for the second tension test in that only one station of strain gages was used. That location was approximately 24 in. (610 mm) north of the center of the iPVC™ fitting. The strain gage station was equipped with 8 strain gages, located at the 12, 3, 6, and 9 o´clock positions (crown, east springline, invert, and west springline,

Table 3.2. Instrumentation for Second Tension Test of iPVC™ Fitting

Location	Instrument Description	Local Instrument Name
24 in. North of Centerline	Crown, Bi-Axial Strain	24CC 24CA
	Invert, Bi-Axial Strain	24IC 24IA
	East, Bi-Axial Strain	24EC 24EA
	West, Bi-Axial Strain	24WC 24WA
Pipe Clamp, 3 in. North Crown of Centerline	Horizontal String Pot	3C_HSP
Pipe Clamp, 3 in. North Invert of Centerline	Horizontal String Pot	3I_HSP
Pipe Clamp, 3 in. North East of Centerline	Horizontal String Pot	3E_HSP
Pipe Clamp, 3 in. North West of Centerline	Horizontal String Pot	3W_HSP
Pipe Clamp, -3 in. South Crown of Centerline	Horizontal String Pot	-3C_HSP
Pipe Clamp, -3 in. South Invert of Centerline	Horizontal String Pot	-3I_HSP
Pipe Clamp, -3 in. South East of Centerline	Horizontal String Pot	-3E_HSP
Pipe Clamp, -3 in. South West of Centerline	Horizontal String Pot	-3W_HSP
Magnet clamp, North End-cap	Horizontal String Pot	N_Slip
Magnet clamp, South End-cap	Horizontal String Pot	S_Slip
Threaded Rod, South Restraints	Horizontal String Pot	Pipe_Stretch
North End-cap	Flow Meter	Flow Meter
Testing Deck	Pressure Transducer	Pressure_Deck
North End-cap	Pressure Transducer	Pressure_Pipe
Actuator	Actuator Displacement	MTS_Disp_IN
Actuator	Actuator Displacement	MTS_Disp_EX
Load Cell	Force Transducer	Force

respectively). Both longitudinal and circumferential strains were measured at each gage location. The instrumentation included an additional string pot to measure the deformation across the specimen from the north to south grip locations.

3.6. Internal Pressure for Second Tension Test

Figure 3.7 presents the pressure plotted relative to time. Initially the pressure spiked to nearly 90 psi (620 kPa), then air was bled from the test specimen. In the plot, various labels and arrows are used to show when various aspects of the test occurred. After the test was started, when the MTS displacements began, the pressure fluctuated from approximately 75 psi (516 kPa) to 80 psi (550 kPa). During the application of tensile displacements, the iPVC™ fitting and adjoining pipes

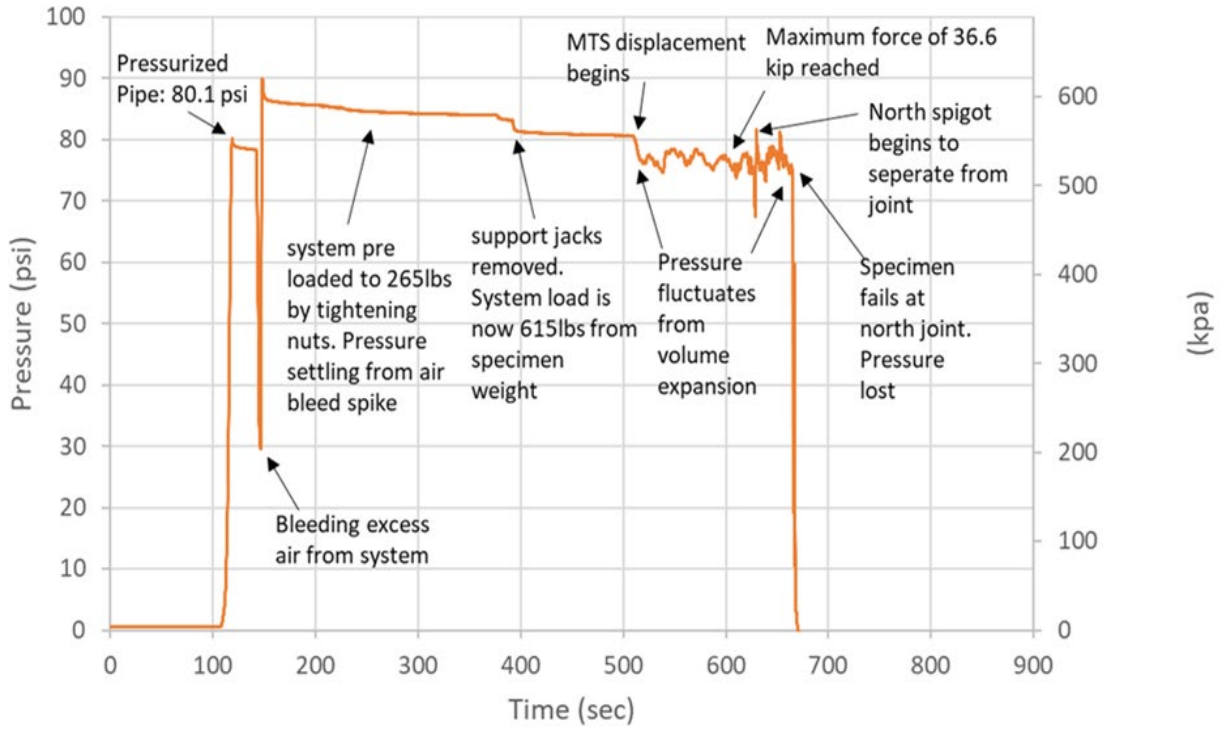

Figure 3.7 Internal Pressure vs. Time for Second Tension Test

expanded axially and thus reduced the pressure. In response, the pressure was increased automatically by the flow meter through the introduction of additional water, providing an average pressure of about 77 psi (530 kPa). At the end of the test, the spigot pulled past the north joint seal, causing leakage and rapid loss of pressure.

3.7. Force and Displacement for Second Tension Test

Like Figure 3.4, Figure 3.8 presents a plot of the load vs. net displacement of the iPVC™ fitting north joint, for which net displacement is the same as that for the first tension test. It is the displacement corrected for the elastic elongation of the pipe between the locations of the string pot anchors and the gripping teeth of the iPVC™ fitting. The elastic displacement correction to obtain the net displacement is very small, and similar in magnitude to that of the first tension test. The net displacement is the actual movement of the north joint without any elastic extension of the pipe and iPVC™ fitting. Virtually all the net movement was concentrated at the north joint.

Labels for various events are presented in Figure 3.8 A maximum load of 36.6 kips (162.9 kN) occurred at approximately 0.7 in. (18.0 mm). Unlike the first tension test, no crack formed along

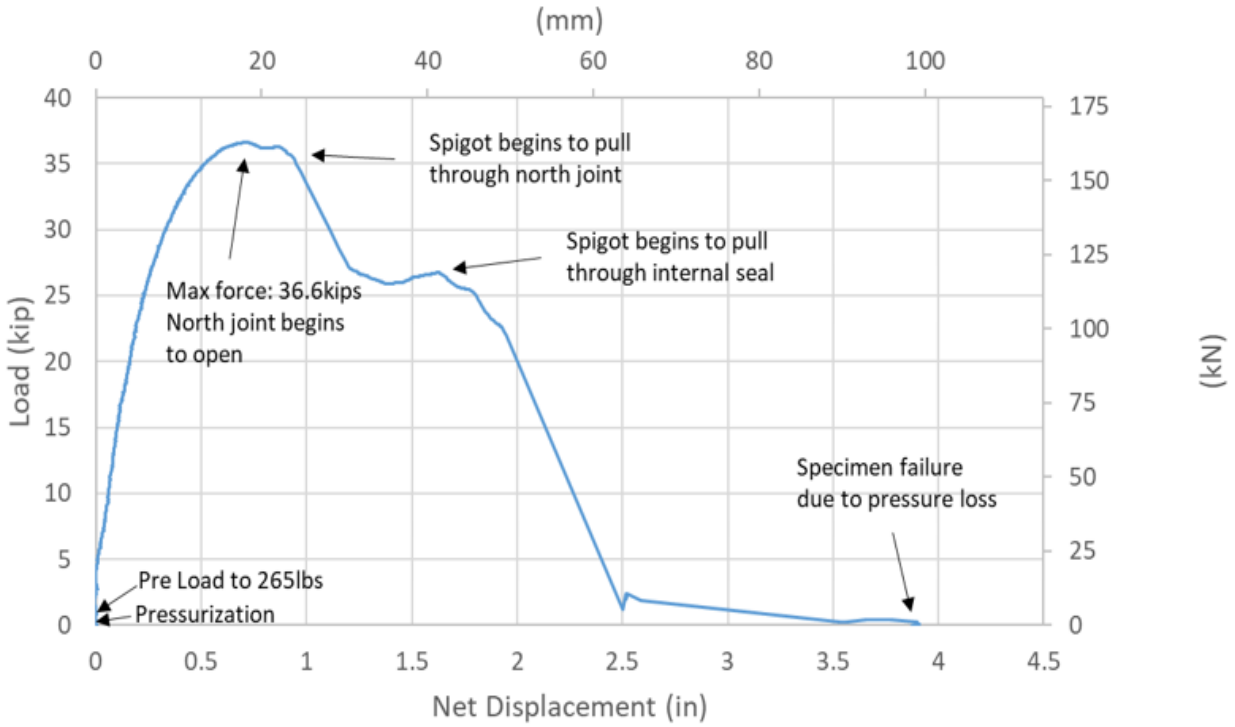

Figure 3.8 Axial Load vs. North Joint Net Displacement for Second Tension Test

the knit line of the iPVC™ fitting. A close examination of the data and video of the iPVC™ fitting during testing shows that movement occurred rapidly from about 2.5 in. (64 mm) to approximately 3.8 in. (97 mm). The north spigot pulled past the gasket in the north coupling of the iPVC™ fitting, when substantial and uncontrollable leakage occurred. This displacement is consistent with dimensions presented in Figure 2.1 that show a distance of about 3.64 in. (92.5 mm) between the end of the spigot and the middle of the gasket. North joint net displacement of approximately 3.8 in. (97 mm) was actually measured when high leakage started. This movement was large enough to carry the end of the spigot past most of the gasket in the north joint.

Figure 3.9 shows the leaking and failed iPVC™ fitting, looking west. All teeth pulled off the barrel of the spigot leaving a white residue. At failure, the teeth were located inside the bell of the north joint. There was a small crack at the knit line of the north joint of the iPVC™ fitting, but it did not penetrate though the joint wall like that of the first tension test. Accordingly, higher normal force and resistance to pullout were generated during the second tension test. The gasket maintained its pressure seal until the end of the spigot was displaced to the outside end of the gasket.

Figure 3.9 Photo of Leaking iPVC™ Fitting for Second Tension Test

3.8. Strains and Forces for Second Tension Test

As previously discussed, strain gages were located and a distance 24 in. (610 mm) north of the iPVC™ fitting center. The strains of the second tension test compare very closely with those of the first tension test. Strain gage readings clearly showed preloading, pressurization, axial tension, and reduction in pressure to zero. The stresses were consistent with theoretical stresses, assuming linear elastic properties as summarized by Price et al. (2018).

3.9. Comparison of Results from First and Second Tension Tests

Figure 3.10 compares the loads vs net displacement of the north joint of the iPVC™ fitting for both the first and second tension tests. The shape of both plots is similar, although the maximum force for each test is significantly different. The force peaks for both tests at approximately the same north joint net displacement. The maximum force is lower for the first tension test because the specimen cracked along the knit line of the iPVC™ fitting. When cracked the circumference of the bell was able to expand more than that of the second tension test. More load normal to the

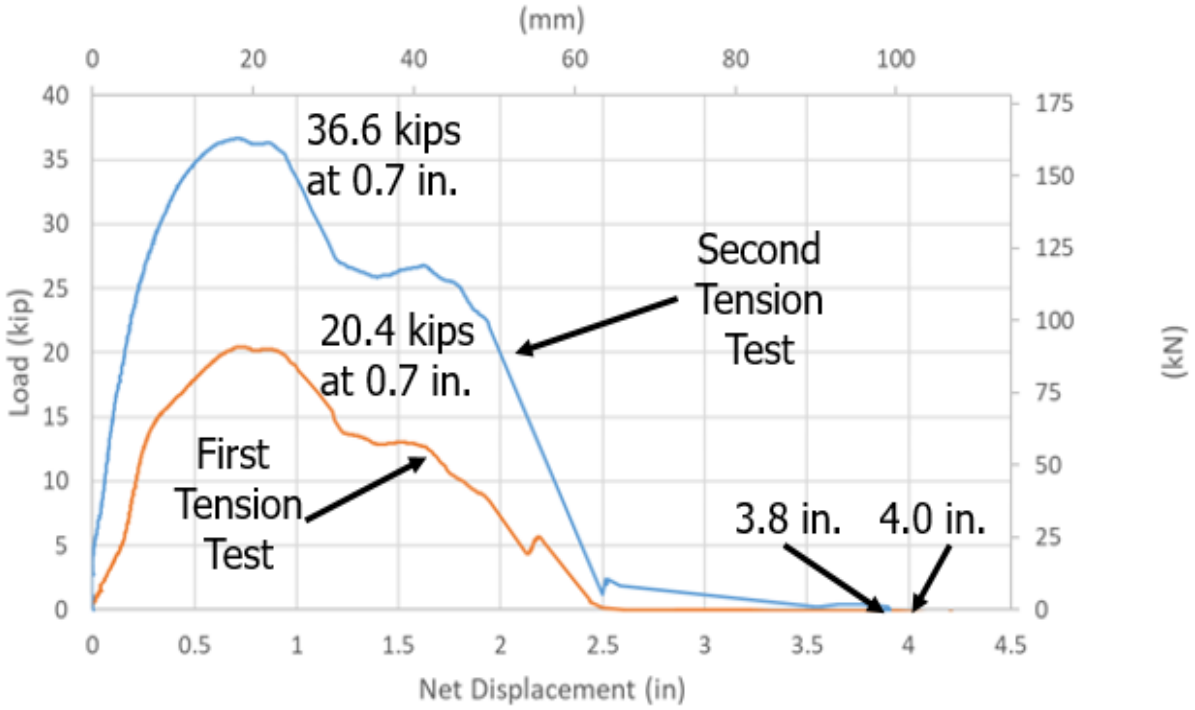

Figure 3.10. Load vs North Joint Net Displacement for First and Second Tension Tests

spigot was able to be carried by the second tension test, which was accompanied by greater pull-out force.

The maximum axial stress in the first and second tension tests was 2.04 ksi (14.1 MPa) and 3.66 ksi (25.2 MPa), respectively. These stresses correspond to 26 % and 47% of the maximum tensile strength of the iPVC pipe, as presented in Table 2.1, for the first and second tension test, respectively. The spigot pulled approximately 4.0 in. (102 mm) and 3.8 in. (97 mm) from the bell of the north joint for the first and second tension test, respectively. At this displacement the pipe failed and began to leak in an uncontrolled way.

Most of the movement occurred at the north joint. The south joint had net displacements of 0.35 in. (8.9 mm) and 0.50 in. (12.7 mm) for the first and second tension tests, respectively. These movements were approximately an order of magnitude smaller than the north joint displacements.

Section 4
iPVC™ Fitting Compression Test

This section summarizes the results of the direct compression test of the iPVC™ fitting, joined to two iPVC pipe specimens. The compression test was performed under internal water pressure that is typical of water distribution systems. Similar to the tension tests, this test is used to evaluate axial compression capacity as well as the load vs. displacement characteristics of the iPVC™ fitting connected to two iPVC pipes.

4.1. Set Up for Tension Test

Figure 4.1 shows a plan view of the setup and equipment for the axial compression test. The orientation of the test specimen is shown with respect to north (N) and south (S). The test set up is similar to that of the tension tests, and the reader is referred to Section 3.1 for a detailed description. The main differences in the setups for the compression and tension tests were the direction of the actuator movement, way in which load was conveyed to the specimen, and stabilization of the specimen.

Tensile force was conveyed from a 55-kip (245-kN) MTS actuator through gripping collars very near both the north and south ends, whereas compressive force was conveyed through special end caps at each end of the test specimen. The end caps also provided for internal pressurization during loading. As shown in Figure 4.1, fixed rollers were located at the north and south pipes to stabilize the specimen against beam buckling. In the field, the iPVC™ fitting and adjoining pipe would be constrained by the adjacent soil against beam buckling.

A photo of the test setup is shown in Figure 4.2. The photo provides a wider perspective than that of Figure 3.2. It shows the data acquisition system, actuator, load cell, iPVC™ fitting and gripping collars on both the north and south sides of the iPVC™ fitting. A detailed description of the gripping collars, instrumentation, and test procedures is given in Section 3.1. The instrumentation is identical to that listed in Table 3.1.

A flow meter was used to monitor the ingress and egress of water with respect to the test specimen. The test was performed under displacement control. The loading rate was 1 in. (25 mm)/min., and the data sampling rate was 5 Hz. Displacement was applied until the specimen was no longer capable of holding internal water pressure.

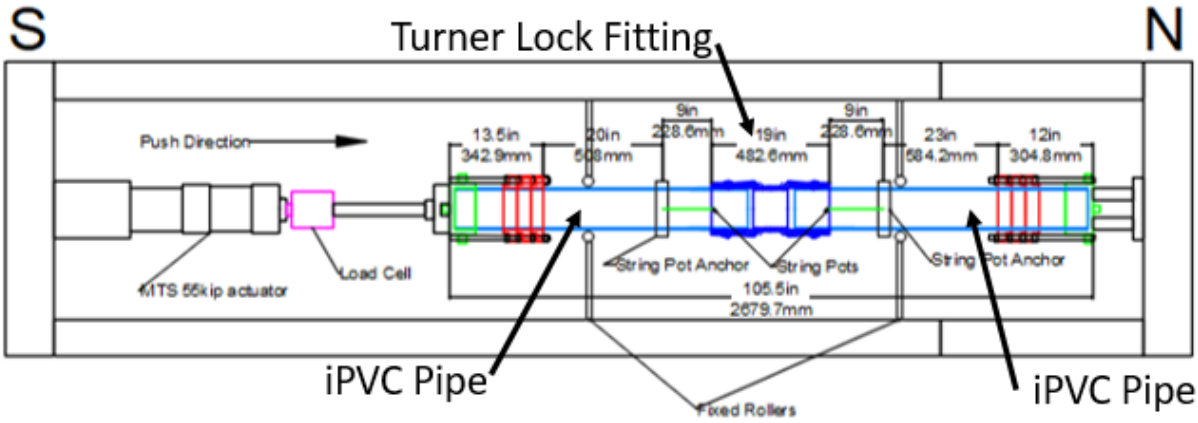

Figure 4.1. Plan View of Axial Compression Test

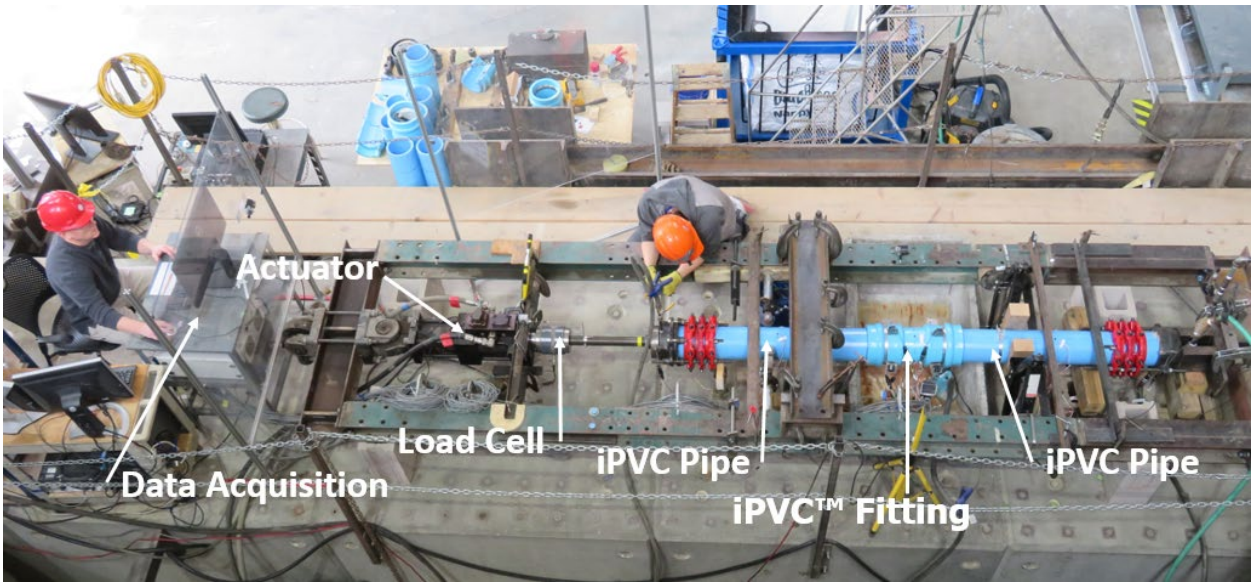

Figure 4.2. Test Specimen in the Direct Compression Frame

4.2. Internal Pressure for Compression Test

Figure 4.3 presents the pressure plotted relative to time. In the plot, various labels and arrows point to different episodes in the pressurization and iPVC™ fitting response. The pressure was initially applied at approximately 80 psi (550 kPa). In response to compressive displacement and axial shortening of the test specimen, the pressure increased to approximately 97 psi (667 kPa), where it was held at a relatively constant value and monitored by the flowmeter. The pressure dropped precipitously when the specimen failed.

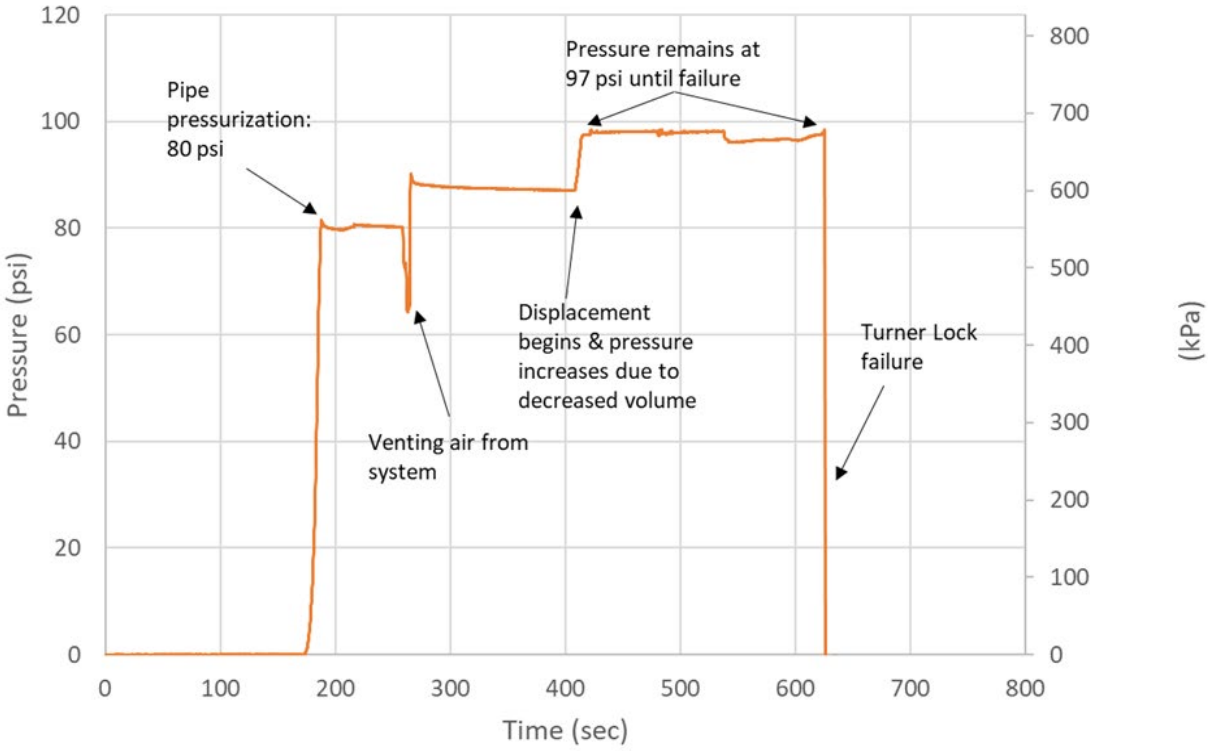

Figure 4.3 Internal Pressure vs. Time for Compression Test

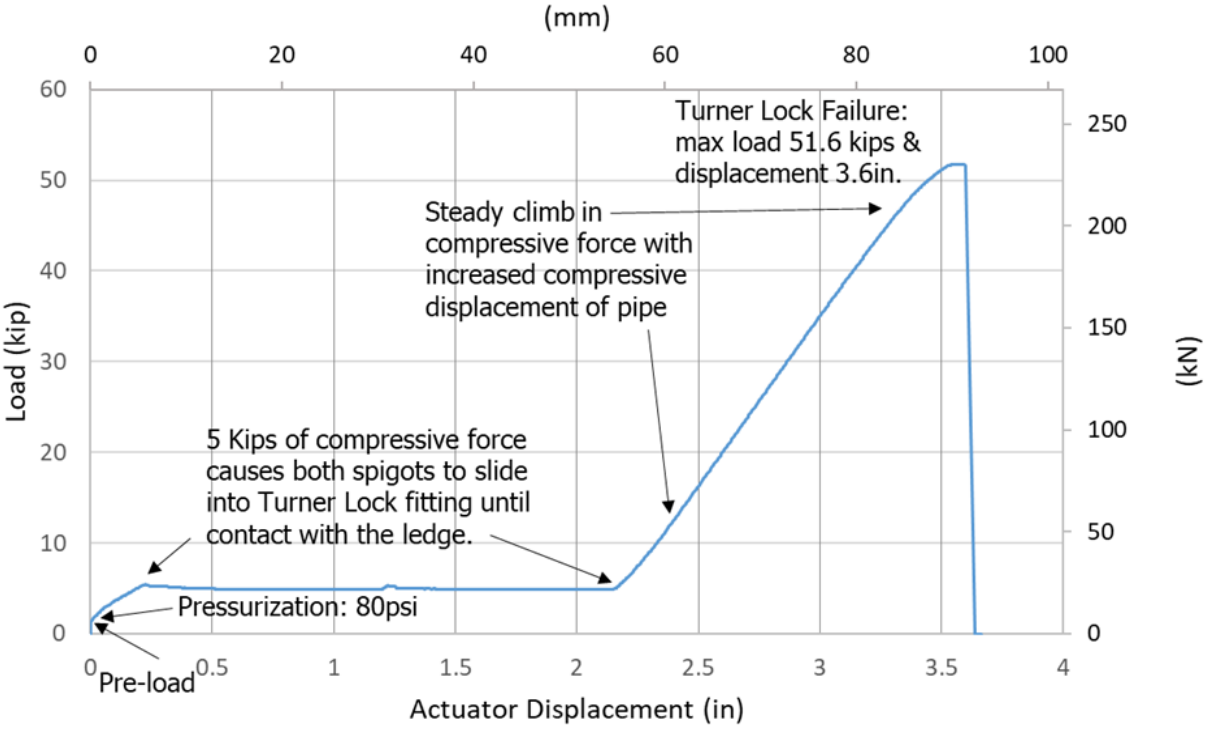

Figure 4.4 Axial Load vs. Actuator Displacement for Compression Test

4.3. Force and Displacement for Compression Test

Figure 4.4 presents a plot of the load vs. actuator displacement. Labels for various events are presented in the figure. Axial loads and displacements associated with preloading and pressurization are shown. At a load of 5 kips (22 kN) both the north and south spigots slid forward in the iPVC™ fitting until further penetration was stopped when each spigot made contact with a ledge in both the north and south portions of the iPVC™ fitting. The axial load then increased from 5 kips (22 kN) to a maximum of 51.6 kips (230 kN) at a displacement of approximately 3.6 in. (91 mm). At this combination of load and displacement, the iPVC™ fitting failed.

The actuator displacement involves 1) spigot penetration into the north and south joints of the iPVC™ fitting, 2) compression of the test specimen, and 3) machine displacement. The machine displacement in turn is composed primarily of a small compression of the actuator/load frame system as well any slip of the gripping collars. The machine displacement was on the order of 0.1in. (2.5 mm) to 0.2 in. (5.0 mm).

As shown in Figure 4.4 there was a total spigot slip of approximately 2.2 in. (56 mm) into the north and south joints of the iPVC™ fitting. Then, there was an additional displacement of 1.4 in. (36 mm) caused by axial compression of the test specimen. This compression was accompanied by a steady increase in load from 5 kips (22 kN) to a maximum of 51.6 kips (230 kN). If the stress vs strain relationships in Figures 2.3 and 2.4 are used, one can calculate a strain of 0.001 associated with 5 kips (22 kN) and a strain of 0.015 associated with 51.6 kips (230 kN). Multiplying the net strain of 0.014 by the 105.5-in (268-mm) length of the test specimen results in approximately 1.5 in. (38 mm) of displacement, which is very close to the measured displacement of 1.4 in. (36 mm).

Figure 4.5 provides a photo of the iPVC™ fitting that failed during the compression test. As shown by Figure 4.4, the iPVC™ fitting failed suddenly in a brittle manner with a rapid decrease in load at 3.6 in. (91 mm) of actuator displacement. The photo shows that the iPVC™ fitting fractured into several pieces with a large piece having fallen below the test specimen.

Figure 4.6 is a profile view of an iPVC™ fitting, where the spigot has pushed into the iPVC™ to make contact with the ledge of the fitting. Load concentrating on the ledge leads to sudden failure. Increased capacity in compression could be attained by providing more distance for the spigot to slid into the iPVC™ fitting joint. In addition, increased compressive displacement capacity could

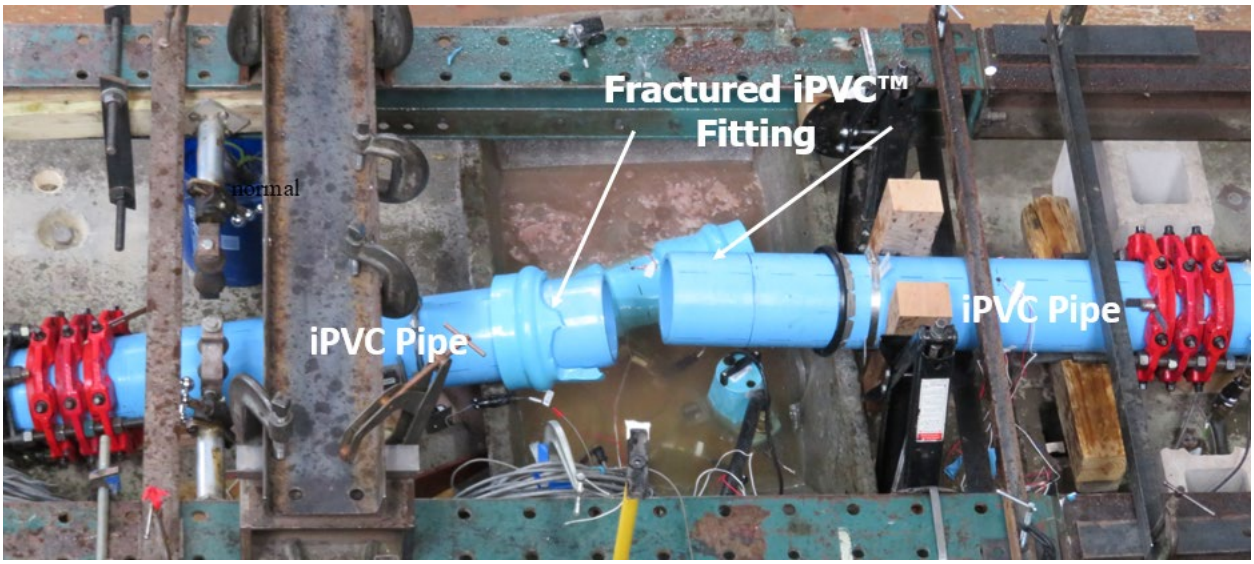

Figure 4.5 Photo of Failed iPVC™ Fitting for Compression Test

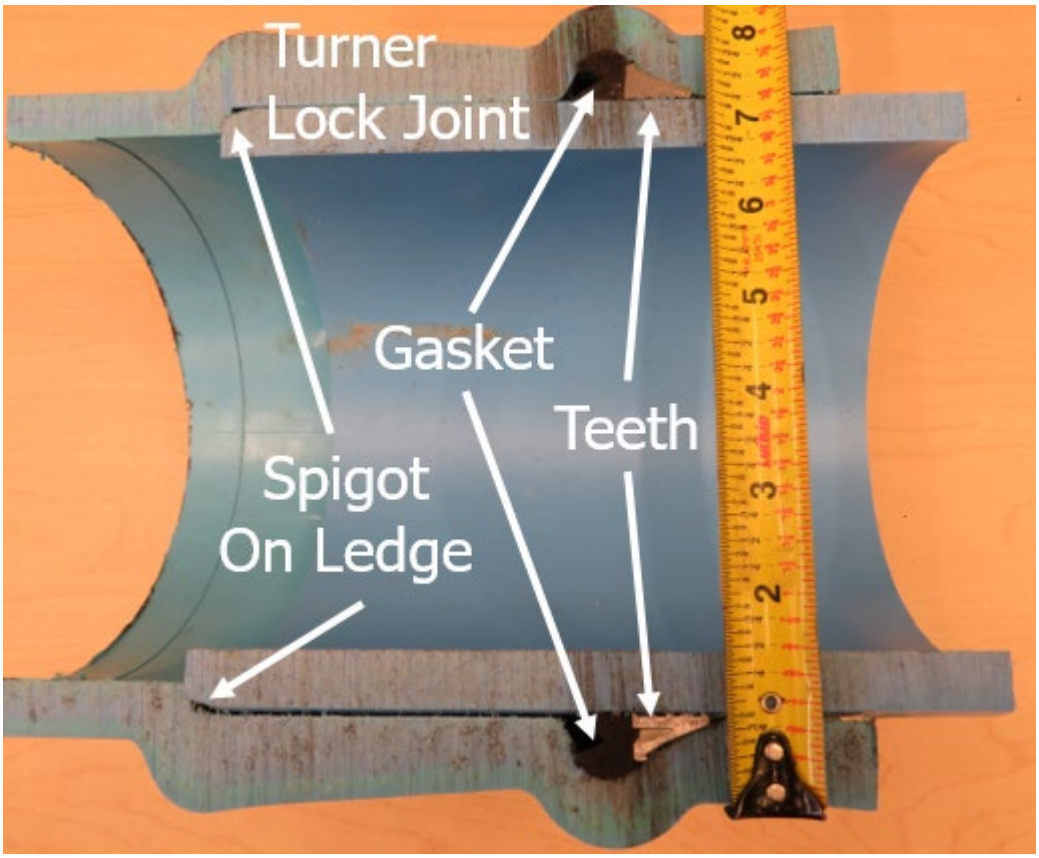

Figure 4.6 Longitudinal Profile of iPVC™ Fitting under Compression

be attained by reducing or eliminating the area of contact at the ledge so that the spigot moves into the central part of the fitting. If the end of the spigot was beveled further, initial contact with the ledge could be reduced or eliminated, resulting in additional compressive displacement capacity.

4.4. Strains and Forces for Compression Test

Similar to the first tension test, strain gages were located at the center of the iPVC™ fitting and at distances both 24 in. (610 mm) north and south of the iPVC™ fitting center. Strain gage readings were converted to stresses that clearly showed preloading, pressurization, axial tension, and reduction in pressure to zero. The stresses were consistent with theoretical stresses, using the stress vs. strain characteristics presented by Price et al. (2018).

Section 5

Summary

Large-scale direct tension and compression tests at Cornell demonstrate the ability of iPVC pipe with iPVC™ fittings to accommodate significant, abrupt ground displacement, including fault movement. The amount of ground movement that can be accommodated with iPVC pipe and iPVC™ fittings will depend on several factors, including the depth of burial, soil type, and the number and spacing of joints relative to the location of abrupt ground movement. Ground movement is accommodated by axial displacement at the iPVC™ fitting joints and either compressive or tensile deformation of the iPVC pipe.

The compression or tension strains of the iPVC pipe are significant. They contribute to the axial movement that is sustained by the iPVC pipe. To help estimate such displacements, Appendix A evaluates the displacement of a pipe centered strike slip fault crossing, as shown in Figure A.1. Details of the analyses are provided in the appendix, and only the salient features of the modeling are provided here. It is assumed that all strains are within the linear elastic limit. The pipeline is buried 4 ft (1.2 m) in medium to dense sand. As the pipeline with iPVC™ fittings is subjected to compression or tension, it deforms. Because it is buried in granular soil, frictional forces are mobilized along the pipeline that resist deformation. By superposition, the elastic longitudinal compressive displacement of the pipeline is simply the maximum compression of the 20-ft (6.1-m)-long center pipe, where all pipe stresses are linearly elastic, minus the elongation of the central pipe due to fiction mobilized along the center pipe.

The compression test shows that compressive joint displacement of approximately 2.2 in. (56 mm) occurs before the spigots make contact with ledges inside the joints. Additional pipe deformation occurs as linear elastic displacement of about 1.4 in. (36 mm). The total compressive displacement that can be accommodated is 3.6 in. (91 mm) over a pipe length of 20 ft (6.1 m), or approximately 1.5% axial compressive strain.

As indicated in Appendix A, 1.4 in. (36 mm) is the estimated elastic displacement for both compressive and tensile stresses induced by abrupt ground, or fault, movement. The elastic displacement is added to the net displacement in Figure 3.10 to obtain the axial load vs tensile displacement plot associated with each load imposed on the pipeline. For example, a tensile displacement of 1.4 in. (36 mm) over a 20-ft (6.1-m)-long pipe is compatible with a 36.6-kip (163-

kN) peak load in the second tension test (see Figure 3.10) at an axial displacement of about 0.7 in. (18 mm) to 0.9 in. (23 mm). Adding 1.4 in. (36 mm) to 0.9 in. (23 mm) results in 2.3 in. (58 mm), which is the displacement that can be accommodated at a tensile axial load of 36.6 kips (163 kN). Please note that the net displacement in Figure 3.10 occurs at only the north joint.

One can generate a plot of the total tensile displacement from the plot for the second tension test by adding to that plot the elastic displacement compatible with each load from 36.6 kips (163 kN) to zero. As shown in Figure 3.10, maximum displacement occurs at zero axial load, as the spigot of an iPVC pipe is being pulled through the gasket of the iPVC™ fitting. As has been previously described, the maximum tensile displacement is the distance between the end of the spigot and the middle of the joint gasket. This displacement is about 3.8 in. (97 mm) over a pipe length of 20 ft (6.1 m), or approximately 1.6 % axial tensile strain.

A strain capacity of 1.5% (compression) to 1.6% (tension) is large enough to accommodate the great majority (91- 92%, respectively) of liquefaction-induced ground strains measured by high resolution LiDAR after each of four major earthquakes during the Canterbury Earthquake Sequence (CES) in Christchurch, NZ (e.g., Bouziou, et al., 2015; O'Rourke, et al., 2014). To put the CES ground strains in perspective, liquefaction-induced ground deformation measured in Christchurch exceed those documented in San Francisco during the 1989 Loma Prieta earthquake (e.g., O'Rourke and Pease, 1997; Pease and O'Rourke, 1997) and in the San Fernando Valley during the 1994 Northridge earthquake (e.g., O'Rourke, 1998). They are comparable to the levels of most severe liquefaction-induced ground deformation documented for the 1906 San Francisco earthquake, which caused extensive damage to the San Francisco water distribution system (e.g., O'Rourke and Pease, 1997; O'Rourke, et al., 2006).

The deformation that can be accommodated by a pipeline with Turner Lock fittings is related to the geometry of the fitting. Additional compressive strain (>1.5%) can be sustained by making the distance longer from the end of the spigot to the ledge in the joint. Removing the ledge will delete a major restraint against the spigot penetrating the fitting, and thus provide for additional compressive deformation. Additional tensile strain (>1.6%) can be sustained by making the distance longer from the end of the spigot to the middle of the joint gasket.

References

Bouziou, D., T. D. O'Rourke, M. Cubrinovski, and D. Henderson (2015) "Evaluation of Ground Deformations during the 2010-2011 Canterbury Earthquake Sequence", *Proceedings*, 6th Intl. Conf. on Earthquake Geotech. Engr., Christchurch, NZ, 8p.

Jung, J.K., T. D. O'Rourke, and C. Argyrou (2016) 'Multi-Directional Force-Displacement Response of Underground Pipe in Sand" Canadian Geotechnical Journal, Vol. 53, pp. 1763 – 1781.

O'Rourke, T. D. (1998) "An Overview of Geotechnical and Lifeline Earthquake Engineering", *Geotechnical Special Publication No. 75*, ASCE, Reston, VA, Proceedings of Geotechnical Earthquake Engineering and Soil Dynamics Conference, Seattle, WA, Aug. 1998, Vol. 2, pp.1392-1426.

O'Rourke, T. D. and J. W. Pease (1997) "Mapping Liquefiable Layer Thickness for Seismic Hazard Assessment", *Journal of Geotechnical Engineering*, ASCE, New York, NY, Vol. 123, No.1, January, pp. 46-56.

O'Rourke, T. D., A. Bonneau, J. Pease, P. Shi, and Y. Wang (2006) "Liquefaction Ground Failures in San Francisco", *Earthquake Spectra*, EERI, Oakland, CA, *Special 1906 San Francisco Earthquake*, Vol. 22, No. 52, April, pp. S91-S112.

O'Rourke, T.D., J.K. Jung, and C. Argyrou (2016) "Underground Pipeline Response to Earthquake Induced Ground Deformation", *Soil Dynamics and Earthquake Engineering*, Vol. 91, pp. 272-283.

O'Rourke, T.D., S.J. Druschel, and A.N. Netravali (1990) "Shear Strength Characteristics of Sand-Polymer Interfaces," *Journal of Geotechnical Engineering*, ASCE, Vol. 116, No. 3, March, pp. 451-469.

O'Rourke, T. D., Jeon, S-S., Toprak, S., Cubrinovski, M., Hughes, M., van Ballegooy, S., and Bouziou, D. (2014) "Earthquake Response of Underground Pipeline Networks in Christchurch, NZ", *Earthquake Spectra*, EERI, Vol. 30, No.1, pp. 183-204.

Pease, J. W. and T. D. O'Rourke (1997) "Seismic Response of Liquefaction Sites", *Journal of Geotechnical Engineering,* ASCE, New York, NY, Vol. 123, No. 1, Jan., pp. 37-45.

Price, D., B. Berger, T.D. O'Rourke, H.E. Stewart, B.P. Wham, and C. Payiya-Ekkasut (2018) "Performance Evaluation of iPVC Pipe under Earthquake-Induced Ground Deformation", Cornell University, School of Civil and Environmental Engineering, Ithaca, NY, Dec.

Appendix A

Elastic Displacements for Pipe Centered Fault Crossing

To help evaluate the elastic components of pipeline displacement one can consider a pipe centered strike slip fault crossing, as shown in Figure A.1. The pipeline is subject to abrupt fault rupture. The pipeline joints are the locations of iPVC™ fittings, which can extend under tension and reduce in length under compression. The pipeline crossing is shown for a right lateral strike slip fault with displacement, d_T, that places the pipeline in compression. The lateral offset is $d_T \sin \beta$, where β is the angle between the pipeline and fault, as shown in the figure. Longitudinal displacement, 1/2 $d_T \cos \beta$, occurs in the pipeline on each of the left and right sides of the fault. Experimental results at Cornell for a jointed pipeline at a pipe centered fault crossing shows that lateral offset causes rotation of the center pipe.

There is relative displacement between the pipe and soil along the center pipe, which generates lateral force per unit distance, p_H. Beyond the joints closest to the pipeline/fault intersection, there is no relative lateral displacement between the pipe and soil. For these conditions an at-rest or K_o pressure exists, p_{Ko}, which acts normal to the pipeline and generates frictional resistance.

It is assumed that the pipeline is buried in granular soil with a friction angle, $\phi = 40°$ at a depth to the top of pipe of 4 ft (1.2 m). The center pipe is 20-ft (6.1-m) long. The pipeline is above the water table. The ratio between the depth to pipeline centerline, H_C, and the iPVC pipe external diameter, D, is $H_C/D = 8$. For both dense dry and partially saturated medium dense sand, as well as the pipe burial depth and external diameter in this example, Jung et al. (2016) show that $N_{qH} = 15$. The apparent frictional force per unit distance, $(p_H)\tan\delta$, which is distributed along the center pipe, is given by

$$p_H \tan\delta = N_{qH} \gamma H_C D \tan\delta = f_A \qquad \text{(A.1)}$$

in which p_H is the horizontal reaction force per unit length between the pipe and soil, δ is the angle of friction between the iPVC pipe and soil, γ is the soil unit weight = 116 pcf (17 kN/m^3), and f_A is the apparent longitudinal frictional force per unit length. O'Rourke et al. (1990) show that $\delta/\phi = 0.6$ for sand in contact with PVC pipe.

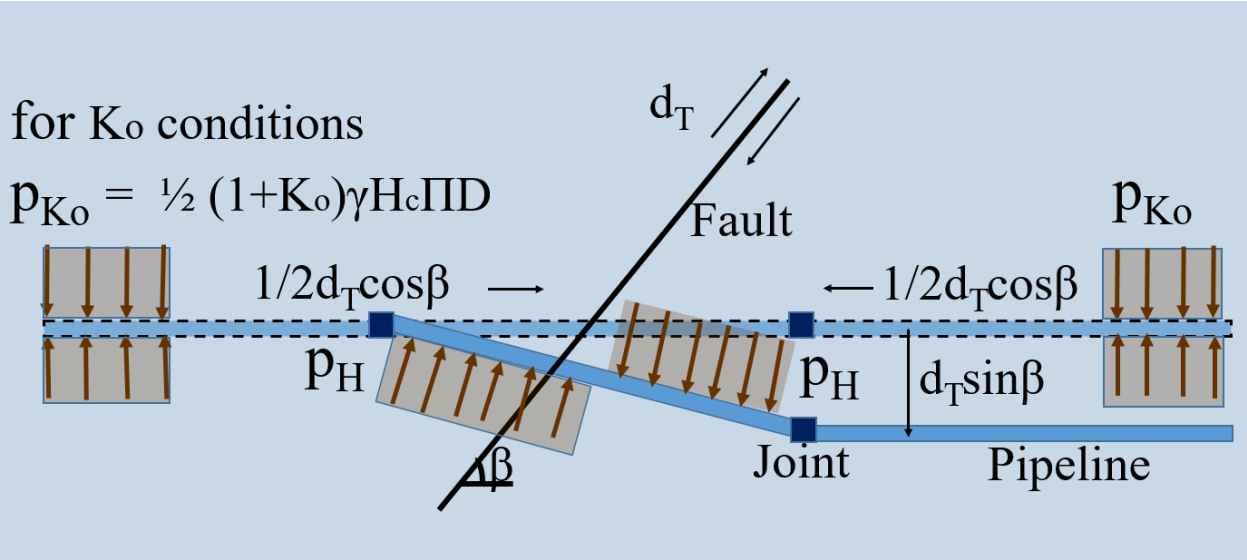

Figure A.1 Plan View of Pipe Centered Fault Crossing

On the basis of full scale experiments, O'Rourke et al. (2006) show that

$$f_T = f_A\left(\frac{1.652}{1.346 + 0.576\tan\delta}\right) \tag{A.2}$$

Combining Eqns. A.1 and A.2 provides the actual, or "true", frictional force per unit distance, f_T. For the properties summarized above, f_T = 0. 149 kips/in. (0.026 kN/mm).

It is assumed that f_T acts predominantly over the center pipe so that f_T effects are disregarded outside the iPVC™ fitting couplings on either side of the center pipe. It is further assumed that f_T is mobilized at a relative slip that is negligibly small. Both these assumptions have little effect on the calculated, longitudinal pipe displacement, and are conservative. By superposition, the elastic longitudinal compressive displacement of the pipeline is simply the maximum compression of the center pipe, where all pipe stresses are linearly elastic, minus the center pipe elongation due to friction mobilized along the pipeline. The elastic compressive displacement of the pipeline, δ_E, is given by

$$\delta_E = \left(\frac{2\sigma_P l}{E}\right) - \left(\frac{f_T l^2}{AE}\right) \tag{A.3}$$

in which σ_P is the proportional limit stress for iPVC pipe ≈ 3.5 ksi (24 MPa), l is the half length of the center pipe = 10.0 ft (3.05 m), E is the Young's modulus = 450 ksi (3.10 GPa) of the iPVC

pipe, and A is the cross-sectional pipe area = 10 in.^{2} (6450 mm^2). For the properties summarized throughout this appendix, δ_E = 1.39 in., say 1.4 in. (36 mm).

Eqn. A.3 applies for both compressive and tensile stresses in the linear elastic range. Thus, δ_E = 1.4 in. (36 mm) is the estimated elastic displacement for both compressive and tensile stresses induced by fault movement.